ZnO microcolumns originated from self-assembled nanorods

Y. Li · W. F. Li · G. Xu · X. L. Ma ·
H. M. Cheng

Abstract ZnO microcolumns originating from self-assembled ZnO nanorods have been prepared by thermal evaporation method at 1,160 °C in a high-temperature tube furnace. The composition and microstructure of as-synthesized products were characterized by X-ray diffraction, scanning electron microscopy, and transmission electron microscopy. It is found that the as-synthesized product consists of ZnO microcolumns with a hexagonal wurtzite structure. The growth direction of the ZnO microcolumns is along the normal direction of $(10\bar{1}2)$ lattice plane of hexagonal structure, while ZnO nanorods that constitute the former are along [0001] direction. Based on the structures' analysis, the possible growth mechanism of ZnO microcolumns originating from nanorods was discussed. Photoluminescence and Raman studies have also been carried out for the ZnO microcolumns and normal commercial powders at room temperature. The discrepancy between Raman and PL spectra of ZnO microcolumns and commercial powders may attribute more relative defects in the microcolumns.

Introduction

ZnO is a promising luminescent material and used for various applications, such as vacuum fluorescent displays owing to its wide band gap (3.37 eV), large exciton-binding energy (60 meV), non-linear optical property, and room ultraviolet emission [1]. It has been used for transparent conductive films, varistors, solar cell windows, and bulk acoustic wave devices [2–4]. Recently, synthesis of one-dimensional (1D) or quasi-one-dimensional nanomaterials is driving for their potential technological application in many different areas including catalysis, microelectronic components, high-performance ceramic and sensors [5–9]. Thus, ZnO 1D nanostructures such as nanowires, nanobelts, nanotubes, and nanorods have been prepared for their excellent and unique properties that can be used in all kinds of devices [10–12]. Several approaches have been developed for the synthesis of ZnO nanostructures including use of metal as catalyst, use of porous alumina templates, and self-assembly of nanostructures (without use of catalyst and template) [13–17]. Unlike other methods, the self-assembly method is simple and more useful. The well-aligned ZnO arrays have been obtained by this method without any confinement of space and direction. Actually, the self-assembled ZnO arrays can be synthesized from several practical approaches including pulsed laser deposition, chemical vapor deposition, and so on [16, 17]. However, to our knowledge, the nanorods constituting a macroscopical integer by self-assembly are unclear.

In this work, we report that ZnO microcolumns originating from self-assembled nanorods have been prepared via a simple thermal evaporation of ZnS powders in a high-temperature tube furnace. X-ray diffraction (XRD) pattern verified that the as-synthesized product was composed of ZnO with wurtzite structure. Scanning electron microscopy (SEM) and transmission electron microscopy (TEM) observations reveal that the ZnO microcolumns originated from the assembled nanorods. The structure details of microcolumns and the growth mechanism were discussed. The characteristic Raman spectra and photoluminescence

Y. Li (✉) · W. F. Li · G. Xu · X. L. Ma · H. M. Cheng
Shenyang National Laboratory for Materials Science, Institute of Metal Research, Chinese Academy of Sciences, Wenhua Road 72, Shenyang 110016, P.R. China
e-mail: yingli3@gmail.com

(PL) spectra of the microcolumns and commercial powders have been measured. The discrepancy between the spectra of the microcolumns and the commercial powders indicated more relative structure defects in the microcolumns.

Experimental

A horizontal alumina tube (outer diameter: 8.1 cm, inner diameter: 7.1 cm, length: 98 cm) was mounted inside a high-temperature tube furnace. Zinc sulfide (15 g, 99%) powders were placed in an alumina crucible. After transferring the crucible to the center of the alumina tube, the tube was evacuated by a mechanical rotary pump to a pressure of 8 Pa. During the experiment, a constant flow of Ar was maintained at a flow rate of 30 SCCM(standard cubic centimeters per minute) and the pump continually evacuated the system so that the pressure inside the tube was kept at 1.4×10^4 Pa. The temperature of alumina tube was slowly increased from room temperature to 1,160 °C and held at this temperature for 2 h before cooling the furnace back to room temperature. After the furnace was cooled down, it was found that white needle-like products were formed on the upper side of the inner wall of the crucible. The composition and morphology of as-deposited products were characterized using X-ray diffraction (Bruker D8 with Cu Kα radiation) and Philips XL 30 FEG scanning electron microscope. Low-magnification images, selected area electron diffraction (SAED), and high-resolution electron microscopy (HREM) images of the as-deposited products were taken on a JEOL-2010 transmission electron microscope. The characterized Raman spectroscopy gained from Jobin Yvon LabRam HR800 was excited by a 632.8 nm laser. Room-temperature PL spectrum was measured on a Hitachi F-4500 fluorescence spectrophotometer equipped with a Xe lamp.

Results and discussion

The XRD pattern shown in Fig. 1 reveals the crystal structure and composition of the as-synthesized products. All main diffraction peaks can be indexed to be of wurtzite ZnO with lattice parameter of a = 3.249 Å, c = 5.206 Å; also some weak peaks near the noise level were not indexed. The strongest peak (102) and the second and third strong peaks (110) and (002) showing the possible preferential growth direction occur along these three lattice planes. SEM observation (Fig. 2) shows the morphology and structure of the as-synthesized product. Figure 2a is an image of several ZnO microcolumns indicating that the lengths of microcolumns are about several centimeters and with a width about 200 μm. Figure 2b is a magnified image
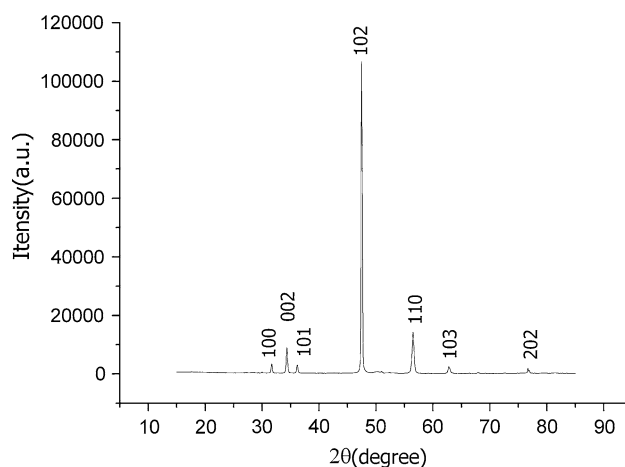

Fig. 1 X-ray diffraction pattern of the as-synthesized products showing that the products consist of wurtzite ZnO
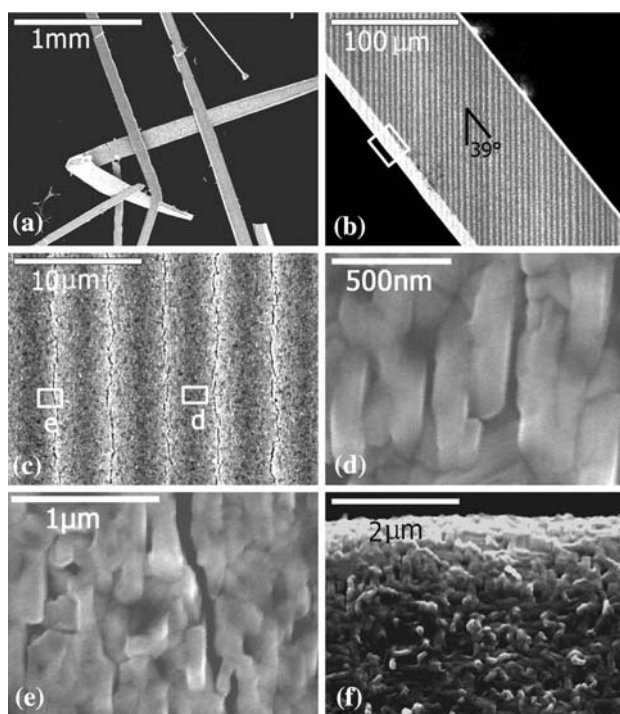

Fig. 2 (**a**) A SEM image of several ZnO microcolumns, (**b**) magnified image of a ZnO microcolumn marked by an arrow in (**a**), (**c**) further magnified image corresponding to middle zone of the microcolumn in (**b**), (**d**) and (**e**) magnified partial images corresponding to the zone marked by two rectangles in (**c**) showing that the as-synthesized products consist of a large quantity of nanorods, (**f**) magnified image corresponding to the boundary zone marked by a rectangle in (**b**)

of the nanorod marked by an arrow showing the large clear straight striped structures existing in the middle part of the microcolumn. The angle between the striped structures and the boundary is 39°. From this image, we also called the microcolumn "microbelts" or "microprisms" but the width

and thickness are close in size. Further magnification of the middle part of image in Fig. 2b is shown in Fig. 2c which reveals that the striped structures are constituted of paralleled ridges and grooves. Figure 2d and e is a magnified partial image corresponding to the zone marked by two rectangles in Fig. 2c showing that the as-synthesized product consists of a large quantity of nanorods. All the nanorods are not fully parallel to the groove and have departure of 2–3°. Figure 2f is a magnified partial image corresponding to the boundary zone marked by a white rectangle in Fig. 2b. Clearly, the array of the nanorods is anomalous in the boundary of the microcolumn. A white thin amorphous layer adheres to the outermost layer of the ZnO microcolumn.

The as-synthesized ZnO microcolumns were ground to powders by an agate pestle. TEM samples were prepared by dispersing the powder in alcohol by ultrasonic treatment and then dropping them onto a porous carbon film supported on a copper grid. Figure 3a is a TEM image of several nanorods; the inset is SAED pattern with incident beam parallel to $[1\bar{2}10]$ direction of ZnO from the area enclosed by a circle in one of several nanorods. The diameters of these nanorods are about several hundred nanometers and the lengths are 4–5 times that of the diameter. The growth direction of the nanorod is along [0001] of the hexagonal structure. Figure 3b shows an HREM image corresponding to the partial zone enclosed by a circle in Fig. 3a, and the characteristic (0001) lattice plane was signed.

As to the formation mechanism of the microcolumns, a schematic illustration of possible growth process is given in Fig. 4a. Because some oxygen gas can leak into the reaction chamber, ZnS can be oxidized into ZnO molecules [18]. Owing to the directional air flow and lattice plane energy, a large quantity of ZnO builds up to a nanorod along [0001] direction. Van der Waals' forces of the molecules on the surface of two nanorods lead to the regular arrangement of plentiful nanorods and finally self-assemble to form a bundle. When the bundle of nanorods
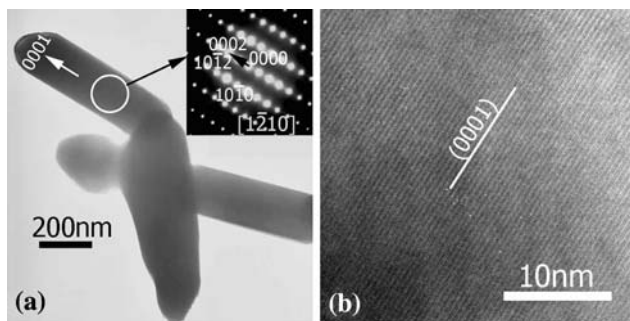

Fig. 3 (a) TEM image of several nanorods, the inset is SAED pattern from the area enclosed by a circle in a nanorod, (b) HREM image corresponding to the zone enclosed by a circle in (a)
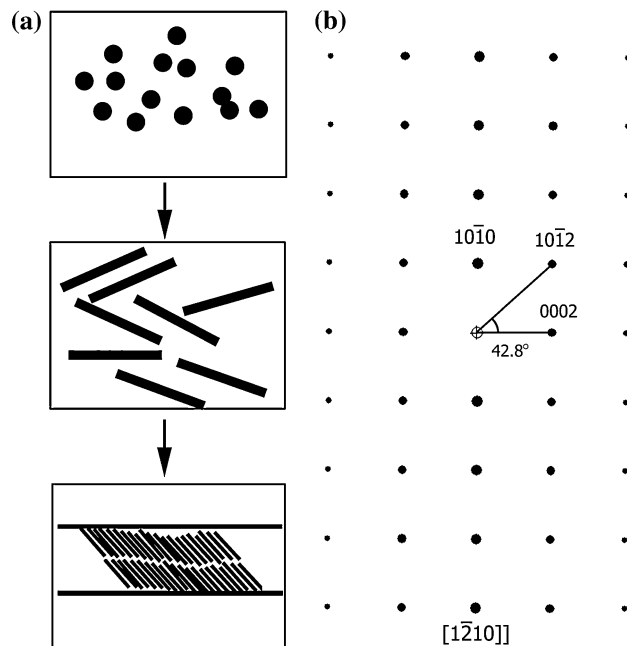

Fig. 4 (a) Schematic illustration showing the possible growth process of a microcolumn, (b) simulated SAED pattern of lattice direction $[1\bar{2}10]$ showing that the angle between $(10\bar{1}2)$ and (0002) plane is 42.8°

reached the limit of length and diameter, the later nanorods joined to the range start to break the rule. Thus irregular nanorods and some amorphous ZnO start to adhere to the surface layer of the ZnO microcolumns, and finally the microcolumns are formed. Figure 4b gives a simulated SAED pattern of lattice direction $[1\bar{2}10]$ showing that the angle between the $(10\bar{1}2)$ and (0002) plane is 42.8°. Combining the above result that the angle between the striped structures and the boundary is 39° and all nanorods are not parallel to the groove but have departure of 2–3°, it is not difficult to confirm that the angle between the macroscopical growth direction of the microcolumn and the nanorod is about 43°. Namely, the macroscopical growth direction of the microcolumn is along the normal direction of $(10\bar{1}2)$ plane (that signed by three-axes method is (102)); this is the reason that the (102) peak is the strongest in XRD pattern.

Investigation of Raman spectrum of the as-synthesized ZnO microcolumns was also performed. For comparison, the Raman spectrum of commercial ZnO powders was also given. As shown in Fig. 5, there are not many differences between the two spectra for ZnO microcolumns and commercial ZnO powders. Two dominating and strong intensity peaks at 96 and 435 cm^{-1}, which are usually observed in the wurtzite-structured ZnO, are attributed to the low- and high-E_2 mode of non-polar optical phonons, respectively [19–21]. Another two small peaks at 330 and 379 cm^{-1} of commercial powders correspond to E_{2H}–E_{2L}
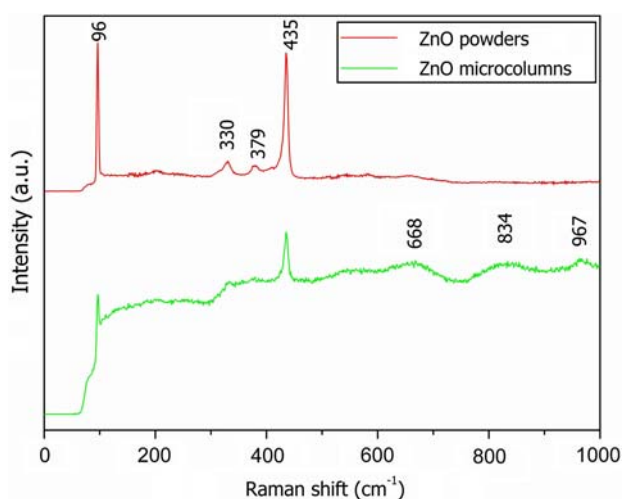
Fig. 5 Raman spectra of the ZnO microcolumns and commercial ZnO powders

and multi-phonon and A_{1T} modes, respectively. In contrast to that, both peaks of ZnO microcolumns are unclear showing a relatively little corresponding scattering mode. The several broad peaks of the ZnO microcolumns are deemed to relate to the interfaces and structural defects (oxygen vacancies and Zn interstitials) of the ZnO microcolumns [22].

The PL spectra of the ZnO microcolumns and commercial powders at room temperature were measured using a xenon lamp as an excitation source at excitation wavelength 325 nm, as shown in Fig. 6. It is clear that the spectrum of commercial powders consists of a sharp and strong emission band located at 384 nm and a weak and broad emission band centered at 493 nm. At the same time, two weak peaks at 451 and 469 nm can be found. Relative to the commercial powders, an obvious red shift of the
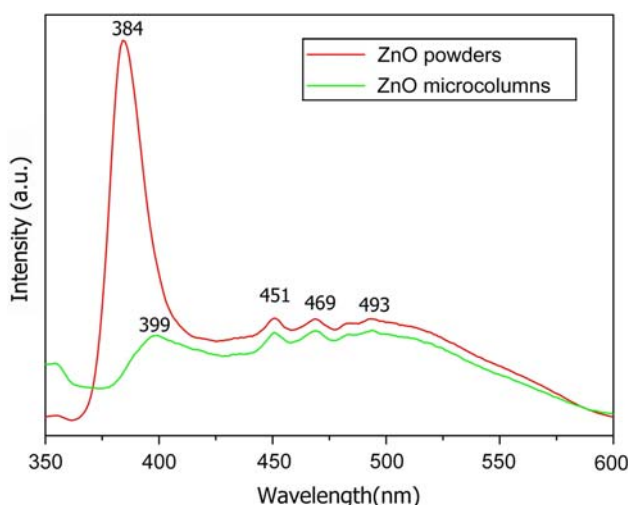

Fig. 6 Room-temperature PL spectra measured from the ZnO microcolumns and commercial ZnO powders

strongest peak occurred, the peak centered at 399 nm and wider than the powders. Instead of this, the other 3 weak peaks almost show no difference from the powders. The near-UV emission at 384 and 399 nm agrees with the band gap of bulk ZnO (around 380 nm), which comes from recombination of free excitation [1, 23]. The red shift of UV emission of the ZnO microcolumns can be attributed to structure defects that reduce energy of free electrons. The other three visible emission peaks can be correlated with the surface/interface defects of ZnO powders and ZnO microcolumns [24, 25].

Conclusion

In conclusion, we have prepared zinc oxide microcolumns originating from self-assembled ZnO nanorods by thermal evaporation method at a temperature of 1,160°. The composition and microstructures of the as-synthesized products were characterized by XRD, SEM, and TEM. The ZnO microcolumns grow along the normal direction of $(10\bar{1}2)$ lattice plane of hexagonal structure, while the nanorods grow along [0001] direction. The main driving forces for the transition from nanorods to self-assembly to microcolumns should be a Van der Waals' force among the molecules on the surface of two nanorods. The discrepant Raman spectra and PL spectra reveal that the ZnO microcolumns originating from nanorods have more structure defects such as oxygen vacancies than normal commercial powders.

References

1. Srikant V, Clarke DR (1998) J Appl Phys 83:5447
2. Yang TL, Zhang DH, Ma J, Ma HL, Chen Y (1998) Thin Solid Films 326:60
3. Cordaro JF, Shim Y, May JE (1986) J Appl Phys 60:4186
4. Verardi P, Nastase N, Gherasim C, Ghica C, Dinescu M, Dinu R, Flueraru C (1999) J Cryst Growth 197:523
5. Pan ZW, Dai ZR, Wang ZL (2001) Science 291:1947
6. Huang MH, Mao S, Feick H, Yan H, Wu Y, Kind H et al (2002) Science 292:1897
7. Owen JHG, Miki K, Bowler DR (2006) J Mater Sci 41:4568. doi: 10.1007/s10853-006-0246-x
8. Li Y, Ma XL (2005) Phys Status Solidi A 202:435
9. Chander R, Raychaudhuri AK (2006) J Mater Sci 41:3623. doi: 10.1007/s10853-006-6218-3
10. Hu JQ, Li Q, Meng XM, Lee CS, Lee ST (2003) Chem Mater 15:305
11. Heo YW, Norton DP, Tien LC, Kwon Y, Kang BS, Ren F, Pearton SJ, Laroche JR (2004) Mater Sci Eng R 47:1

12. Zhao Q, Xu XY, Song XF, Zhang XZ, Yu DP, Li CP, Guo L (2006) Appl Phys Lett 88:033102
13. Huang MH, Wu Y, Feick H, Tran N, Weber E, Yang PD (2001) Adv Mater 13:113
14. Li Y, Meng GW, Zhang LD, Phillipp F (2000) Appl Phys Lett 76:2011
15. Park WI, Kim DH, Jung SW, Yi GC (2002) Appl Phys Lett 80:4232
16. Choopun S, Tabata H, Kawai T (2005) J Cryst Growth 274:167
17. Yan M, Zhang HT, Widjaja EJ, Chang RPH (2003) J Appl Phys 94:5240
18. Yuan HJ, Xie SS, Liu DF, Yan XQ, Zhou ZP, Ci LJ, Wang JX, Gao Y, Song L, Liu LF, Zhou WY, Wang G (2003) Chem Phys Lett 371:337
19. Vanheuseden K, Seager CH, Waren WL, Tallant DR, Voigt JA (1996) J Appl Phys 79:7983
20. Xing YJ, Xi ZH, Xue ZQ, Zhang XD, Song JH, Wang RM, Xu J, Song Y, Zhang SL, Yu DP (2003) Appl Phys Lett 83:1689
21. Yang PD, Yan HQ, Mao S, Russo R, Johnson J, Saykally R, Morris N, Pham J, He RR, Choi HJ (2002) Adv Funct Mater 12:323
22. He FQ, Zhao YP (2006) J Phys D: Appl Phys 39:2105
23. Monticone S, Tufen R, Kanaev AV (1998) J Phys Chem B 102:2854
24. Hu JQ, Bando Y (2003) Appl Phys Lett 82:1401
25. Tong YH, Liu YC, Shao CL, Mu RX (2006) Appl Phys Lett 88:123111